PERGAMON

International Journal of Multiphase Flow 27 (2001) 1881–1901

International Journal of Multiphase Flow

www.elsevier.com/locate/ijmulflow

Using positron emission particle tracking (PEPT) to study nearly neutrally buoyant particles in high solid fraction pipe flow

P.G. Fairhurst [b], M. Barigou [a,*], P.J. Fryer [a], J-P. Pain [c], D.J. Parker [d]

[a] *School of Chemical Engineering, University of Birmingham, Edgbaston, Birmingham, B15 2TT, UK*
[b] *Nestlé Product Technology Centre, CH-1350 ORBE, Switzerland*
[c] *Institut des Sciences et Techniques de Valenciennes, IUP, 6 Rue de Rambouillet, BP 444, 59408 Cambrai, France*
[d] *Positron Imaging Centre, School of Physics and Space Research, University of Birmingham, Edgbaston, Birmingham, B15 2TT, UK*

Received 27 March 2000; received in revised form 20 May 2001

Abstract

Positron emission particle tracking (PEPT) allows the flow path of a tracer particle to be followed in opaque flows. It has been used here to study particle trajectories and velocity profiles of a single radioactively labelled tracer particle in high solid fraction, solid–liquid pipe flow. Experiments studied 5 and 10 mm almost spherical alginate particles, of specific gravity 1.02 in a 45 mm internal diameter pipe positioned either vertically or horizontally. Solid delivery concentrations from 20% to 40% v/v were investigated in carrier fluids of 120–500 mPa s mean apparent viscosity, with mean mixture velocities of 20–125 mm/s. Different flow patterns were identified and studied including concentric and capsule flow. A slow-moving annular region of particles near the pipe wall was measured when high viscous carrier fluids and/or small particles were used. The asymmetry of the horizontal velocity profiles was found to depend strongly on the solid concentration and the particle Reynolds number. Results are especially relevant to food and bioproduct flows but show the relevance of the technique to the study of solids conveying.

Keywords: PEPT; Solid–liquid flow; Velocity profile; Flow patterns; Capsule flow; Concentric flow

* Corresponding author. Tel.: +44-121-4145277; fax: +44-121-4145324.
E-mail address: m.barigou@bham.ac.uk (M. Barigou).

0301-9322/01/$ - see front matter
PII: S0301-9322(01)00038-6

1. Introduction

1.1. Solid–liquid flows in process and food engineering

Solid–liquid mixtures are encountered in various industries. In most cases slurries consist of small particles (up to 1 mm in diameter); however, in gravel or coal slurries and solid–liquid food mixtures particle sizes can be much larger (up to 2 cm in diameter). These mixtures cannot generally be considered as single-phase 'pseudo-fluids' with effective rheological properties, as inertial effects, gravitational forces, particle–particle and particle–wall interactions affect the flow of the solid particles giving rise to different particle behaviours and flow patterns from the carrier fluid. Knowledge of these flow patterns (Doron and Barnea, 1996) is necessary for pressure drop calculations and information about particle behaviour is important when the residence time of particles in tube flow is a factor in process optimisation. In food processing, a number of operations involve the conveying of high solid fraction foods (up to 50% solids) in non-Newtonian carrier fluids at low Reynolds numbers. These foods may be heated and cooled during flow: the rate and extent of reactions that result in microbial sterility, but which also impair quality, depend critically on the flow of the mixture. It is important that every part of the food reaches the correct level of sterility, but not to be over-processed. Understanding the dynamics of two-phase food flows is thus crucial for an efficient design of these operations (see Lareo et al., 1997a; Barigou et al., 1998).

A number of non-intrusive particle flow measuring systems have been used to study solid–liquid flows. These can be classified into two categories: tracer methods which provide Lagrangian type data as the tracer is tracked in space and time; and Eulerian methods which provide local instantaneous information on the flow field, i.e., time series data at a fixed point. Various (Eulerian) optical methods have been employed to determine the velocity profile or residence time of solid particles. Segré and Silberberg (1962a,b) used light beams to determine local particle concentration. Ohashi et al. (1979) used a photographic method to study the local velocities of very small particles ($d = 0.321$–1.84 mm). Later they developed a laser method for measuring local particle concentration and velocity (Ohashi et al., 1980). Laser-Doppler Anemometry (LDA) has been widely used to measure particle velocities (see, for example Fregert, 1995; Averbakh et al., 1997; Shauly et al., 1997). Fregert (1995) studied plastic spheres in horizontal flow, and found that the velocity profile was skewed with the point of maximum axial velocity shifted above the centreline. Okuda (1981) used a camera with a stroboscope to determine the trajectories of plastic spheres in pipe flow. Dutta and Sastry (1990a,b) used video taping to study the velocity distribution of particle suspensions in simulated holding tube flow. Very low solid concentrations were used (<1%) and qualitative observations concerning particle–particle interactions made.

Recently, other visual methods have been developed for measuring the velocity and radial position of a particle in a solid–liquid pipe flow. The visual technique of particle imaging velocimetry (PIV) has been used in a number of applications including the automobile and food industries (for example, Zitoun, 1996). The velocity profile is measured using small tracers; the flow is then imaged in two perpendicular planes and image analysis methods used to track the paths of the individual tracers and give a vector plot of velocities. Lareo et al. (1997b,c) filmed tracers in solid–liquid food flows using mirrors at 45° to the pipe to enable the radial position to be identified. For concentrations up to 10% three velocity profiles were identified in vertical upflow; partial plug flow in the centre of the pipe, in which the particle velocity is independent of radius, a

parabolic profile where particle velocity varied with radius, and a combination of the two. Circumstances were found under which particle migration across streamlines took place.

The above visual methods are generally simple but have limited applications as low solid concentrations (up to about 10%), transparent carrier fluids and pipe walls are necessary. Commercial flows use much higher solid fractions in which visual methods are limited. Magnetic resonance imaging (MRI) can be used to measure the velocity field of opaque solid–liquid mixtures (McCarthy et al., 1997; McCarthy and Kerr, 1998). McCarthy et al. (1997) studied the average horizontal velocity profiles for alginate spheres in Carboxymethylcellulose (CMC) solutions. They found the velocity profiles to be flattened compared with single-phase carrier fluid flow and that profile flattening increased with increasing solid concentration and particle size. Tracking individual particles is not practically possible using MRI, however. The technique yields Eulerian type measurements and, as a result, only an average velocity field can be measured and not individual particle behaviour such as particle velocity or particle migration across streamlines.

Other methods of the Lagrangian type have been used to measure the residence time of a tracer in pipe flow. Toda et al. (1973) used a radioactive technique where γ-ray irradiated particles were used in straight pipes and bends. The particle velocity was determined from its passage time between two scintillation probes. Segner et al. (1989) used EMF sensors in which a small magnet was embedded in the tracer particle which was then detected using copper coils wound around the pipe. These were connected to a small amplifier linked to a potentiometer for detecting the electromotive force. Such a method requires non-metallic tube walls, as does the technique used by Liu et al. (1993) and Lareo (1995). Here, tracer particles wrapped in metallic foil were detected using two copper detection coils around the pipe, connected to an alternating bridge which was disturbed by the passage of a particle. Tucker and Withers (1994) have used Hall effect sensors to measure residence times in an industrial pilot plant; these have the considerable advantage of being able to function through metallic walls. Ultrasonic Doppler Velocimetry (UDV) was developed for fluid flow measurement in opaque systems. It has been successfully used to measure velocity profiles as a function of space and time in various systems such as the pipe flow of water, coal slurry and chocolate (Takeda, 1995). The technique has great potential in the mapping of solid–liquid flows.

The above residence time measurement methods, although they can operate in opaque media, can only measure the average velocity of a particle over a given pipe length and not the radial position, velocity profile or the instantaneous velocity. Positron emission particle tracking (PEPT) is a Lagrangian technique which can be used to track particles continuously through opaque media, as described below. The objective of this study was to apply PEPT to study the flow of large particles in high solid fraction solid–liquid flow, both to determine the applicability of the technique to study hydraulic conveying and to identify flow patterns of relevance to food processing and safety. For the processing of solid–liquid food mixtures, thermal information is needed on the time individual particles spend within the system: PEPT is ideally suited to this type of measurement.

1.2. Positron emission particle tracking

Radionuclides which decay by β^+ decay with the emission of a positron (a positive electron) and make useful tracers since the positron rapidly annihilates with an electron, producing a pair

of 511 keV γ-rays which are emitted almost exactly 'back-to-back'. Coincident detection of these two γ-rays by a pair of detectors defines a line passing close to the point of emission; detection of a number of events makes it possible to identify the point of origin of the signal. This is the basis of the imaging technique of positron emission tomography (PET) often used in medicine. The concentration of the labelled phase can be reconstructed by standard tomographic techniques from the number of γ-ray pairs emerging along each line of sight.

Since 511 keV γ-rays are very penetrating, the technique also has considerable potential for engineering studies. The only system dedicated to engineering applications is the Birmingham University positron camera (Parker et al., 1997). Unlike most medical systems, this consists of a pair of multi-wire proportional chambers each with an active area of 600×300 mm^2 and capable of locating a detected γ-ray to within about 5 mm. The two detectors are placed either side of the system of study and operate in coincidence mode, an "event" only being recorded if the γ-rays are detected by both detectors with a resolving time of 12 ns. The camera data rate is limited to ca 3000 coincidence events per second, so that acquiring sufficient data to enable tomographic reconstruction of an extended tracer distribution may take many minutes. Use of the camera in this way has therefore concentrated on a range of steady-state situations, and applications have ranged from imaging lubricant distribution within an operating jet engine (Stewart et al., 1987) to mapping the concentration of sand grains in a stirred slurry (McKee et al., 1995).

For dynamic studies, the technique of PEPT has been developed (Parker et al., 1993). Here a single labelled tracer is used, the position of which can be determined by triangulation from a small number of detected γ-ray pairs. Many of the detected events are corrupt, for example because one of the γ-rays has been scattered, so location requires acquisition of sufficient events in order that the valid ones, whose reconstructed lines essentially meet at one point, can be distinguished. The actual number of events used depends on various factors, including the tracer speed. In general a slow-moving tracer is located to within ± 2 mm, typically 20 times a second; the method has been generally used to study the mixing and flow of particles within systems such as fluidised beds and powder mixers (Parker et al., 1997). In this case a particle is placed in the mixer and its flow followed for long enough to construct an image of the flow field and the occupation frequency for particles in different positions. Less work has been done on tracing flows, although Fangary et al. (2000) have studied fluid trajectories within a mechanically agitated vessel using the method.

2. Experimental

2.1. Flow loop

To avoid the problem of pumping high solid fraction flows (such as particle disintegration and blockages), and to minimise the complexity of the equipment used within the PEPT laboratory, a gravity driven flow loop was designed and built, as shown in Fig. 1. The solid particles were first kept in suspension in an upper reservoir by a mechanical agitator. The solid–liquid mixture then flowed from the reservoir through two 1400 mm long sections of transparent perspex pipe (45 mm i.d.). One of these, horizontal or vertical depending on which flow geometry was to be studied, was placed between the PEPT detection plates. Joined to the

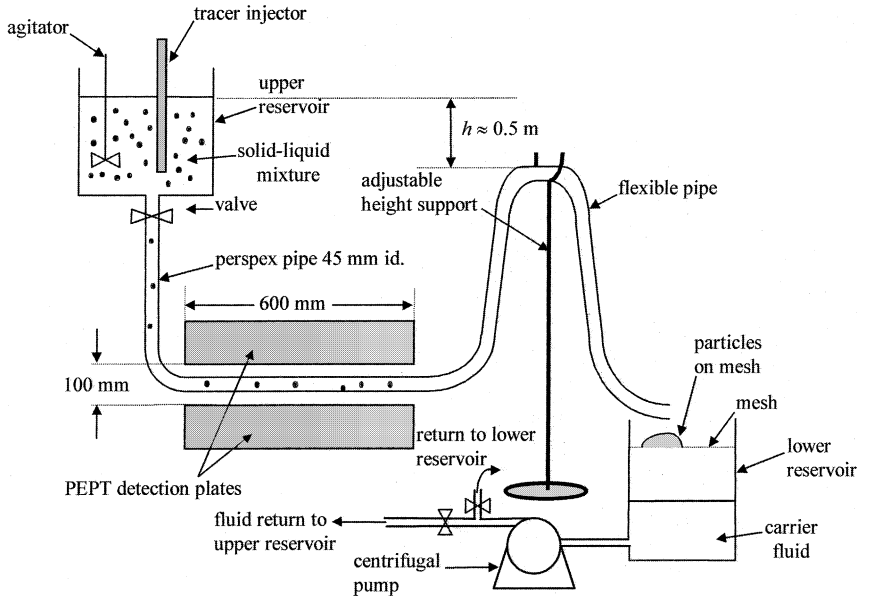

Fig. 1. Experimental flow loop used.

perspex pipe was a length of flexible tubing. This flexible pipe was supported by an adjustable height stand, the height of which controlled the fluid drop distance, h, from the upper reservoir and thus the flow rate of the mixture. The relationship between h and the flow rate was established empirically. The solid–liquid mixture then flowed over a mesh that separated the solid particles from the fluid which then flowed into the bottom reservoir. The solid particles were then collected manually from the mesh and returned to the upper reservoir. The carrier fluid was pumped back into the upper reservoir using a centrifugal pump. At the pipe outlet, the volumetric flow rate and solids delivery concentration were measured several times during each experimental run.

The location of the perspex pipe between the detection plates was measured before and after experimental runs by sticking a radioactive tracer on the tube wall of the perspex pipe at different locations. During an experimental run, tracers were injected into the upper reservoir through a pipe and collected on the lower reservoir mesh, at least 50 particle trajectories were measured in order to obtain a representative sample (Lareo, 1995).

2.2. Range of experiments

CMC carrier fluids (commercial name Blanose Cellulose Gum, type Blanose 7HF, distributor Hercules, Aqualon France) of either 0.5% or 0.8% w/w concentration were used. Their preparation is described by Fairhurst and Pain (1999). These fluids were found to follow an Ellis fluid rheology, thus

$$\mu_a = \frac{\mu_0}{1 + \left(\tau/\tau_{1/2}\right)^{\alpha-1}}, \tag{1}$$

where μ_a is the apparent viscosity, and μ_0, $\tau_{1/2}$ and α are the model parameters (μ_0 is the zero shear viscosity; $\tau_{1/2}$ is a parameter that denotes the shear stress, τ, at which the apparent viscosity has dropped to $\mu_0/2$, and α (>1) is a measure of the extent of shear-thinning behaviour). The Ellis parameters were determined by non-linear curve fitting for the two solutions used and the values are given in Table 1.

The solid particles used were 5 or 10 mm alginate spheres, fabricated on site as described by Fairhurst (1998). Their mechanical properties, density and sedimentation velocities were measured (Fairhurst and Pain, 1999) and are given in Table 2. The alginate particles to be used as tracers were coloured with methyl blue dye, to allow visual identification. A 600 μm resin bead containing the positron emitting radionuclide ^{18}F (half life of 110 min), produced with a ^{3}He beam from a cyclotron, was used as the radioactive tracer. This resin bead was then placed in the tracer particle: tracers were made by drilling a hole in the alginate particle, placing the resin bead in the centre and then filling the hole with alginate solution. The resin bead volume was approximately 2×10^{-7} that of the alginate particle and had no measurable effect on the density of the particle. The tracer thus had the same physical properties (density, mechanical, surface roughness) as any other particle and thus flowed in a similar manner through the system: the particle track is thus representative of the others. Experiments were performed at outlet delivery concentrations of $Cs = 21 \pm 2\%, 30 \pm 2\%, 40 \pm 2\%$ v/v solids and mean mixture velocities from 24 to 125 mm/s. Details of the experiments are given in Table 3.

Preliminary experiments were conducted to confirm that the 90° bend joining the vertical and horizontal pipe sections did not affect flow in the horizontal section of the pipe. The absence of significant entry effects in the horizontal section was tested by comparing particle axial velocity distributions for the first and second halves of the horizontal pipe in the camera's field of view, each section therefore being 250 mm long. Fig. 2 shows the instantaneous axial velocity distribution for 50 particles (experimental conditions: mean mixture velocity, $\overline{v} = 34 \pm 2$ mm/s; volumetric solids delivery concentration $Cs = 21 \pm 2\%$ v/v, 10 mm particles, 0.8% w/w CMC carrier

Table 1
Ellis model parameters for CMC solutions used

CMC concentration (% w/w)	μ_0 (Pa s)	$\tau_{1/2}$ (Pa)	α	R^2 (regression coefficient)
0.5	0.12	6.6	2.03	0.99
0.8	0.62	7.4	2.03	0.99

Table 2
Properties of solid particles used in experiments

Particle diameter (mm)	5 ± 0.4	10.2 ± 0.6
Density (g/cm^3)	1.02 ± 0.006	1.02 ± 0.006
Eccentricity (d_{min}/d_{max})	0.98 ± 0.02	0.97 ± 0.03
Sedimentation velocity (mm/s):		
0.8% w/w CMC	0.40 ± 0.04	0.77 ± 0.1
0.5% w/w CMC	1.8 ± 0.9	4.3 ± 0.5
Force-compression relation (elastic limit = $0.1d$); f(g), x (mm)	$f = 15x^2 + 19x + 5.2 \pm 7\%$	$f = 14x^2 + 31x + 6 \pm 10\%$

Table 3
Range of experimental conditions

Flow direction	Particle diameter (mm)	CMC concn. (% w/w)	Solid delivery concn. (% v/v)	Mixture flowrate (l/h)	Mean mixture velocity (mm/s)	Particle Reynolds no. Re_p	Tube Reynolds no. Re_t
Horizontal	10	0.8	21 ± 2	440 ± 15	77 ± 3	0.012	8.2
				190 ± 10	33 ± 2	0.012	3.0
			30 ± 2	440 ± 14	77 ± 3	0.012	8.2
				160 ± 8	28 ± 2	0.012	2.5
			40 ± 2	440 ± 18	77 ± 3	0.012	8.2
				300 ± 10	52 ± 2	0.012	5.1
				140 ± 8	24 ± 2	0.012	2.1
		0.5	30 ± 2	375 ± 16	65 ± 3	0.075	27.2
			40 ± 2	500 ± 21	87 ± 4	0.075	37.4
	5	0.5	30 ± 2	370 ± 13	65 ± 2	0.075	27.2
			40 ± 2	720 ± 33	125 ± 6	0.075	56.3
Vertical downflow	10	0.5	40 ± 2	720 ± 33	125 ± 6	0.358	56.3
			21 ± 2	410 ± 19	72 ± 3	0.358	30.4
			30 ± 2	390 ± 18	68 ± 3	0.358	28.5
			40 ± 2	375 ± 15	65 ± 3	0.358	27.2

fluid). The two velocity distributions are bimodal and very similar. The means and standard deviations are 32 and 17 mm/s, and 32 and 15 mm/s (for first and second halves, respectively) indicating that any entry effects present do not measurably affect the particle velocity distributions.

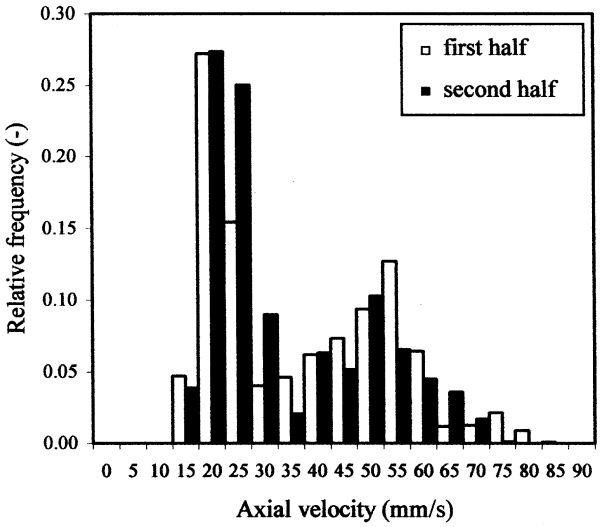

Fig. 2. The absence of significant entry effects: comparison of particle velocity distributions for first and second halves of horizontal pipe.

2.3. Data processing and presentation

The unique aspect of the positron camera is that it can track individual particles through a process. Some plots displaying particle trajectories over a three-second period are presented in this paper. To relate these results to other studies where it is only possible to measure mean velocities requires velocity profiles to be calculated. There is some uncertainty in each PEPT location because the positron travels an unknown distance from the tracer before it meets an electron. This, together with any possible change in radial position of the particle meant that an algorithm was required to calculate the instantaneous velocity of the tracer particle. The algorithm used is explained in Appendix A and gives an unbiased estimate of particle velocities to within ±2.3 mm/s for a tracer moving at a mean velocity of about 40 mm/s, or to an accuracy of ±6% (Fairhurst, 1998). Over an experimental run therefore, the calculated particle instantaneous velocities will have a maximum error equal to

$$\sqrt{(\text{PEPT location error } [6\%])^2 + (\text{variation in flow rate } [4\%])^2},$$

i.e., 7.2% of the mean particle velocity.

Fig. 3 shows how the pipe cross-section has been divided into different zones for the purpose of results presentation and analysis. Particle velocity data are presented in a number of different ways:

(i) As *statistical velocity distributions*. The pipe cross-section is divided into two regions corresponding to radial positions $r < 10$ mm and $r > 13$ mm, as shown in Fig. 3(a), and statistical particle velocity distributions are determined for these two regions. Particles that fell in the

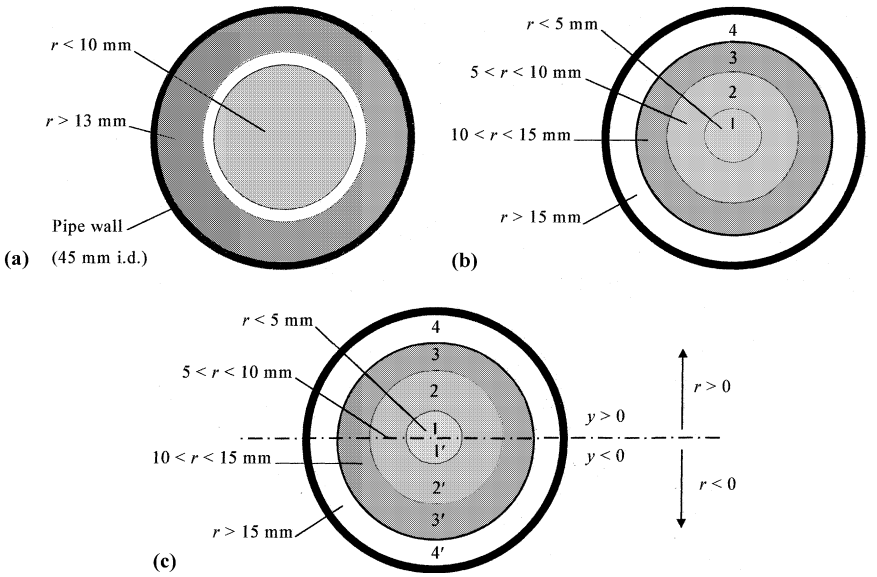

Fig. 3. Division of pipe cross-section for classification of radical velocity profiles and statistical velocity distributions: (a) two flow regions for two-flow-region velocity distribution analysis; (b) four flow regions for "global" velocity profile calculation; (c) eight flow regions for top to bottom velocity profile calculation.

intermediate gap $10 < r < 13$ mm were not included because of the error associated with determining particle radial position. As will be shown later, in Fig. 7, the velocity distributions in these two flow regions can be significantly different.

(ii) As *radial velocity profiles*. The need here is to measure both the radial particle velocity profile and the extent, if any, of radial particle segregation within the pipework. Two different velocity profiles are thus presented:

- *Global* profiles where the mean velocity of particles in the radial regions shown in Fig. 3(b) were calculated. These regions were used in the study of vertical flows, where no radial particle segregation would be expected.
- In horizontal flow, however, radial particle segregation would be expected because of gravitational effects, and particle velocities in the top and bottom halves of the pipe cross-section would be different. *Vertical plane* (or radial) velocity profiles were thus used: the radial regions used to calculate the mean velocity of particles in horizontal flow are shown in Fig. 3(c). The regions above and below the centreline are discriminated: radial positions above the centre are plotted as positive and below the centre as negative.

The asymmetry of the vertical plane profiles in horizontal flow was assessed by comparison with the corresponding global profiles. A skewness parameter ($\overline{s}_n$) was defined, where $\overline{s}_n$ is the square root of the sum of the squares of the velocity differences between vertical plane profiles and global profiles in horizontal flow. For example, for the top half of the pipe cross-section, i.e., for zones 1–4 in Fig. 3(c):

$$\overline{s}_n^2 = \left[v_{\mathrm{np}}(\text{zone 1}) - v_{\mathrm{np}}(\text{zones 1 and } 1')\right]^2 + \left[v_{\mathrm{np}}(\text{zone 2}) - v_{\mathrm{np}}\ (\text{zones 2 and } 2')\right]^2 + \left[v_{\mathrm{np}}\ (\text{zone 3}) - v_{\mathrm{np}}\ (\text{zones 3 and } 3')\right]^2 + \left[v_{\mathrm{np}}\ (\text{zone 4}) - v_{\mathrm{np}}\ (\text{zones 4 and } 4')\right]^2, \quad (2)$$

where each term represents the difference between the mean velocity in a given radial region in the top half of the tube cross-section, and the mean velocity over the same whole radial region including the bottom half; v_{np} is the normalised particle velocity (velocity divided by mean mixture velocity).

3. Results and discussion

3.1. Flow patterns and particle trajectories in horizontal flow

Fairhurst et al. (1999) and Fairhurst and Pain (1999) found that an annular region of slow-moving particles one-particle thick could be identified close to the pipe wall when small particles and/or viscous carrier fluids were used. The criterion for the existence of such annular region was $Re_{\mathrm{p}} < 0.08$, where the particle Reynolds number, Re_{p}, was defined as

$$Re_{\mathrm{p}} = \frac{v_{\mathrm{sed}}^{\infty}\rho_L d}{\mu_0}, \quad (3)$$

where $v_{\mathrm{sed}}^{\infty}$ is the sedimentation velocity of the particle in an infinite expanse of carrier fluid, ρ_L the carrier fluid density, d the particle diameter, and μ_0 is the zero-shear viscosity for an Ellis fluid.

The existence of an annular region is a function solely of particle diameter and carrier fluid rheology and, hence, the definition of Re_p on the basis of particle sedimentation velocity rather than mean particle velocity or mean slip velocity. The presence of this annular region then leads to the formation of two distinct flow regions, a central core of relatively high velocity and an outer annulus containing slower-moving particles. Fig. 4 depicts a set of typical particle trajectories from a horizontal flow of 30% v/v solids ($d = 10$ mm) in 0.8% w/w CMC, which clearly shows these two flow regions: (i) in the centre of the pipe a region close to plug flow exists, in which particles move rapidly and independently at ca 130 mm/s; and (ii) particles closer to the tube wall are slower and travel much less distance within the three-second period represented. Such a flow situation is referred to as concentric flow (Fairhurst et al., 1999). As well as the formation of an annulus, the effect of sedimentation due to gravity is also evident: at the base of the pipe particles in the outer annulus travel at about 65 mm/s whilst at the top of the pipe particles travel at about 100 mm/s.

In the flow situation shown in Fig. 4, little radial migration between flow regions was measured; the particles held more or less the same position as they travelled along the pipe. The line across the pipe shows the distance travelled if particles moved at the mean velocity; in all but the base of the tube, particles occupied spatial positions that allowed them to travel at an axial velocity greater than the mean velocity of the mixture.

At higher solid concentrations (for example, $Cs = 40\%$ v/v) when $Re_p < 0.08$, there is insufficient space to accommodate the spatial configuration of concentric flow with a fast core of

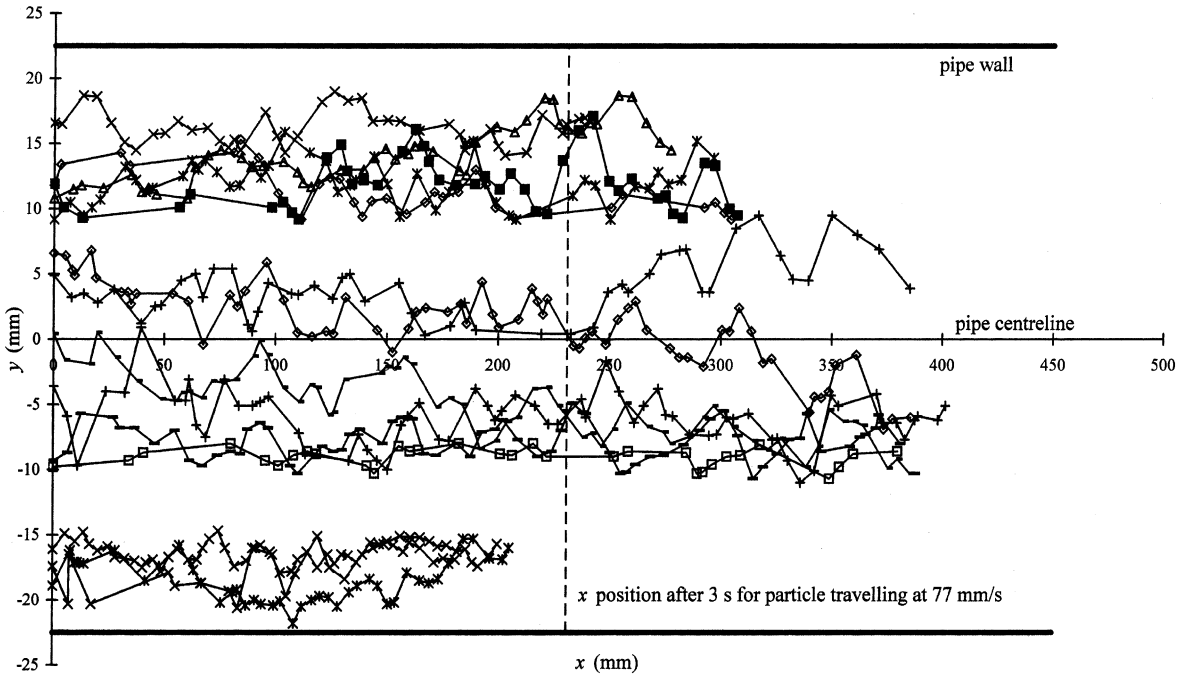

Fig. 4. Three-second particle trajectories in horizontal flow showing two distinct flow regions: 0.8% w/w CMS; $d = 10$ mm; mean mixture velocity = 77 mm/s; $Cs = 30\%$ v/v.

individual particles, and agglomerates referred to as capsules start to form leading to capsule flow. Fig. 5 shows the packing in a ~40% v/v solids flow of 10 mm particles, with an annular region one particle thick surrounding a central core. In this case, the flow consists of slow-moving capsules and particles between these capsules moving much faster. During capsule flow, particles were observed to accelerate downstream off the front of a capsule whilst upstream other fast approaching particles collided into it, thus joining the agglomerate of slow particles. The size of each capsule, therefore, remained approximately the same whilst the individual particles within the capsule changed continuously. The presence of such rapidly moving particles has important implications for food processing as they will be the last to reach the required level of thermal treatment in a given process. The current practice of designing continuous thermal processes assuming that the maximum velocity is twice the average velocity is conservative and can result in losses of nutrients and quality; the fastest particles are much slower than predicted by assuming laminar flow (see Fig. 4). An optimal process should ideally take into account the actual flow regimes established. Thus, a particle would be considered to flow rapidly if it has a velocity significantly greater than the mean mixture velocity. For solid fractions of 30% or more an arbitrary limit of $\sim 1.2\overline{v}$ could be defined. For short processes (e.g. HTST, ca 10 s) the existence of a particle velocity range of approximately $0.9\overline{v} - 1.7\overline{v}$ even for 3 s will lead to a significantly heterogeneous treatment (see Fig. 4).

Typical particle trajectories for a capsule flow are presented in Fig. 6. The effect of the slow outer annulus is again clearly seen, as in Fig. 4, with slower particles near the wall, and the slowest of all in the bottom region of the pipe. In addition, there is significant variation in particle velocity in the centre of the pipe: *slow* particles flowing in the capsules at ca 70 mm/s, close to the mean fluid velocity; and *fast* particles flowing at velocities up to 130 mm/s between the capsules.

Measurements by PEPT yield both the velocity and position of particles; this allows the effect of the division of the pipe cross-section into two distinct flow regions to be seen clearly. The statistical velocity distributions for the core and annulus have been separated using the rules shown in Fig. 3(a): Fig. 7 depicts such velocity distributions for $Cs = 21\%, 30\%$ and 40% v/v solids.

At the lowest solid concentration, in Fig. 7(a), the two distributions are distinct: the fastest particle in the outer region travels at ca 0.9 of the mean velocity, whilst the slowest particle in the central region travels at more than 1.4 times the mean velocity. Some of the particles in the core

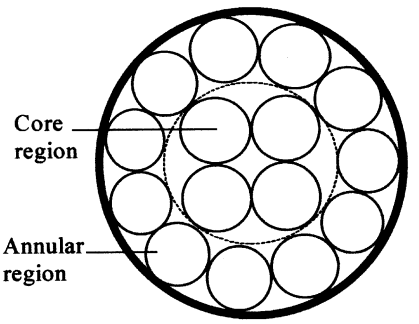

Fig. 5. Filling of pipe cross-section at transition from concentric to capsule flow: a core region surrounded by a one-particle thick annular region; 0.8% w/w CMC; $d = 10$ mm; $Cs \sim 40\%$ v/v.

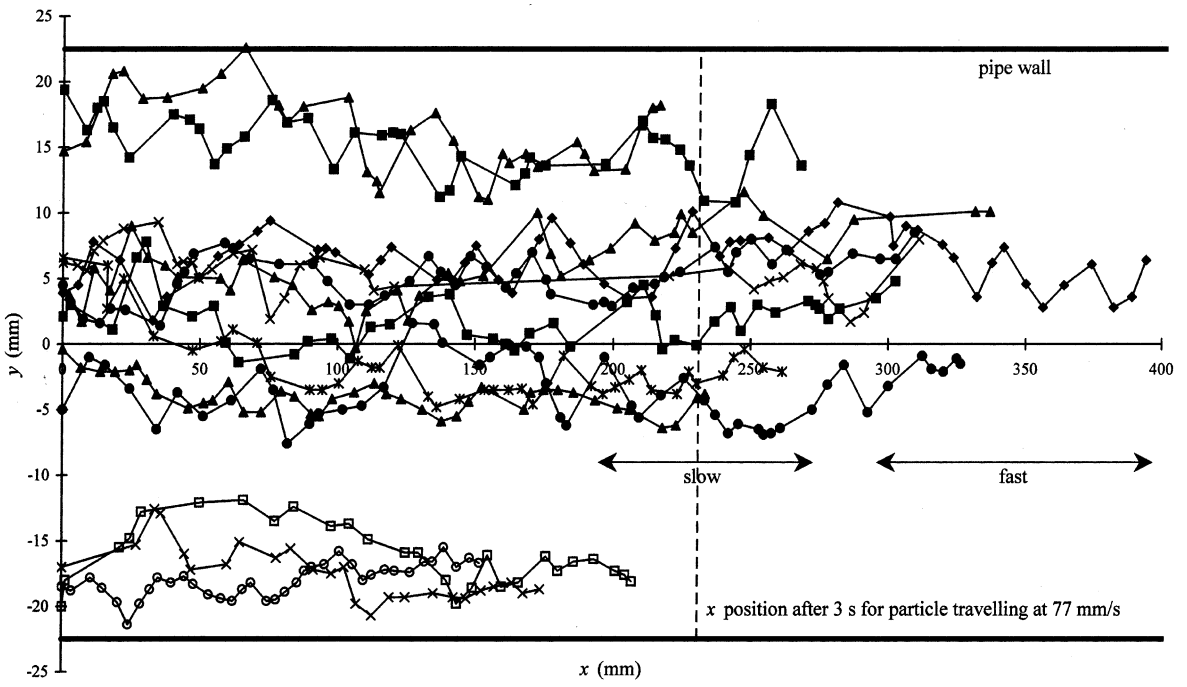

Fig. 6. Three-second particle trajectories showing horizontal capsule flow: 0.8% w/w CMC; $d = 10$ mm; mean mixture velocity = 77 mm/s; $Cs = 40\%$ v/v.

region of the flow travel at more than twice the mean velocity of the flow. Similar behaviour is seen at 30% solids fraction, in Fig. 7(b), although the very high velocities are not seen. As the solids fraction increases, the two distributions come closer together, until at $Cs = 40\%$ v/v, transition to capsule flow occurs and the two velocity distributions overlap.

This type of behaviour has been previously noted, see for example Lareo et al. (1997a,b,c), but the advantage of PEPT is that it can separate the two regions explicitly, and can identify the existence of capsule flow. It is not possible to identify capsule behaviour from velocity profile data alone. This is a significant effect, because food processes are commonly designed on the assumption that the flow is fully developed and Newtonian, i.e., that particles can travel twice as fast as the mean flow. The possibility of this type of capsule flow forming suggests that under certain circumstances this assumption might not be appropriate. As described above, transition from the concentric flow regime to capsule flow regime corresponds to the solid concentration where particle crowding is such that particles can no longer fit into two entirely separate flow regions (Fig. 5).

For conditions where $Re_p > 0.08$, the division of the flow into an annular region and a central region was less obvious. This can be seen in the three-second particle trajectory plot in Fig. 8 which shows a 40% v/v solids flow of 10 mm particles but for a lower CMC concentration of 0.5% w/w – so that the sedimentation velocity is much greater, as shown in Table 2, than for the same size particles in Fig. 6. Under the experimental conditions represented in Fig. 8 gravitational effects are important: a few slow-moving particles can be seen near the bottom of the pipe,

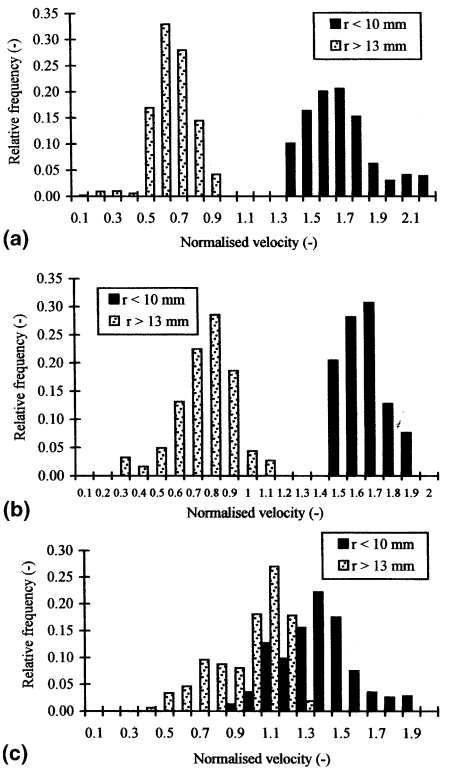

Fig. 7. Effects of solid concentration on normalised velocity distributions in core and annular regions: $d = 10$ mm; 0.8% w/w CMC. (a) $Cs = 21\%$ v/v; mean mixture velocity = 34 mm/s; SD = 18.2 mm/s. (b) $Cs = 30\%$ v/v; mean mixture velocity = 28 mm/s; SD = 10.2 mm/s. (c) $Cs = 40\%$ v/v; mean mixture velocity = 24 mm/s; SD = 6.8 mm/s.

whereas particles at the top of the pipe travel much faster. However, particle trajectory is a much weaker function of particle radial position than in Fig. 6, with no slow moving particles at the top of the pipe. A much smaller capsule effect is seen in the centre of the flow: the range of particle velocities in the central region is 90–130 mm/s. All the particles, bar the ones at the bottom of the pipe, were seen to travel faster than the mean velocity, shown as the dashed line across the pipe in the figure.

3.2. Radial velocity profiles in horizontal flow

Fig. 9 shows the global radial velocity profiles, developed using the definition of Fig. 3(b), for 10 mm particles in 0.8% w/w CMC. The solid lines show the expected profile for the liquid flowing alone, using the Ellis model (Eq. (1)) with the parameter values given in Table 1. As would be expected, the global radial particle velocity profile becomes increasingly flattened as the solid concentration increases; the maximum normalised particle velocity measured, v_{np}^{max}, reduces from 1.7 to 1.4 as Cs increases from 21% to 40%. The mean flow velocity over the central region ($r < 10$ mm) is uniform in both cases. Experimental results similar to those of Fig. 9 have been

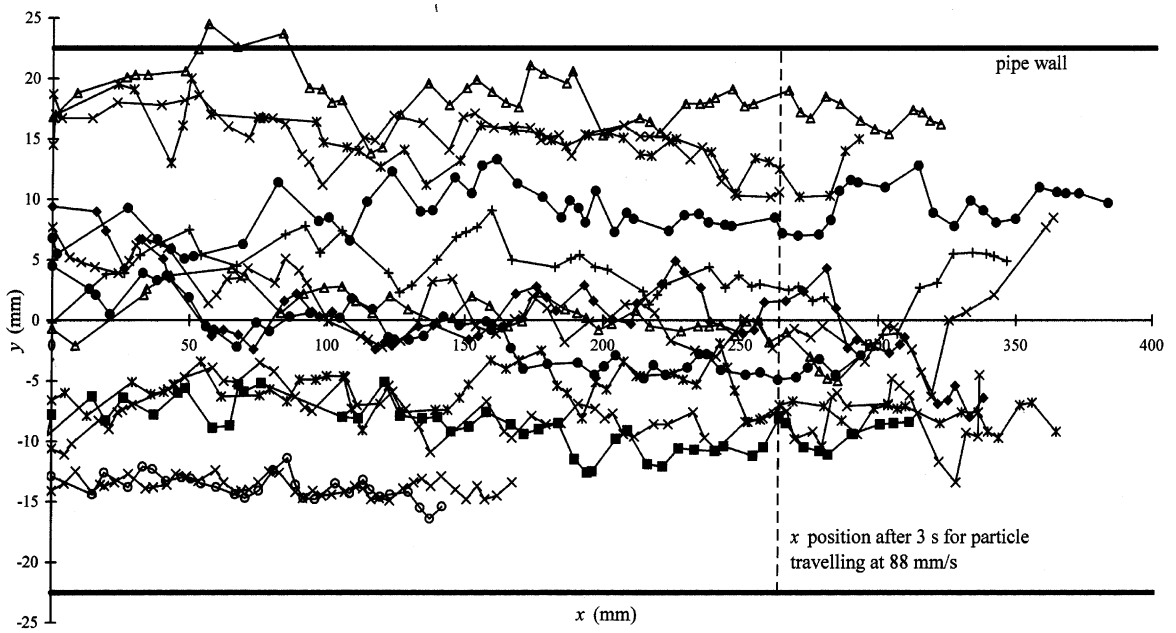

Fig. 8. Three-second particle trajectories showing horizontal capsule flow: 0.5% w/w CMC; $d = 10$ mm; mean mixture velocity = 88 mm/s; $Cs = 40\%$ v/v.

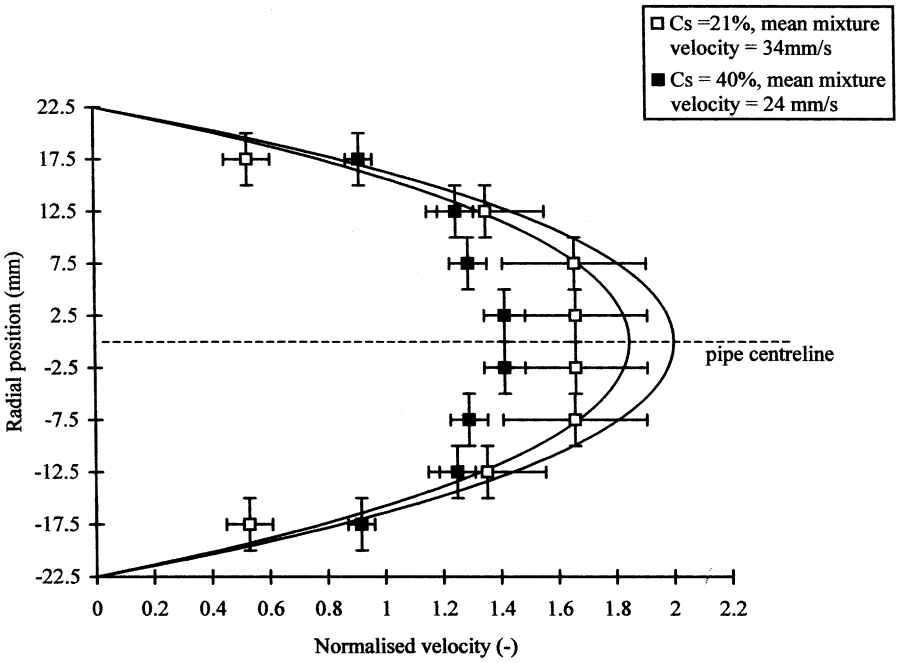

Fig. 9. Global velocity profiles in horizontal flow: solid lines represent velocity profiles for Ellis liquid flowing alone; 0.8% w/w CMC; $d = 10$ mm.

reported by McCarthy et al. (1997) for alginate spheres in CMC solutions, using MRI. The averaged profiles, however, do not reveal the effects of the capsule flow at $Cs = 40\%$.

Increasing the particle size was also found to increase the flattening of the global velocity profiles (data not shown); v_{np}^{max} thus reduced from 1.65 for 5 mm particles to 1.4 for 10 mm particles in 0.5% w/w CMC, for $Cs = 30\%$ and $\overline{v} = 65$ mm/s. This can be explained by the fact that the greater the particle size, the greater the expected interaction between particles, and hence the more uniform the velocity profile.

These global profiles do not reveal the whole picture, however; because of gravitational effects, sedimentation skews the flow patterns between the top half and the bottom half of the pipe cross-section. Fig. 10 represents the vertical plane velocity profiles determined according to the flow regions defined in Fig. 3(c). Here, it can be seen that the velocity profile for the lowest solid concentration ($Cs = 21\%$) is strongly asymmetric with the point of maximum axial velocity shifted about 2.5 mm above the centreline. At $Cs = 40\%$, however, the radial velocity profile is much more symmetrical indicating that gravitational effects are slight; in this case, particle–particle interactions are clearly more significant.

Such asymmetric profiles have been reported for sand and water slurries in hydraulic conveying (for example by Newitt et al. (1962) and many others) and for model food flows of low solid concentration (Fregert, 1995) up to 10% v/v. PEPT allows these flow patterns to be identified in much higher solid fractions than has been seen for food flows.

The degree of asymmetry in the radial velocity profiles measured in horizontal flow was a function of the solid concentration, particle size, mean mixture velocity and carrier fluid viscosity.

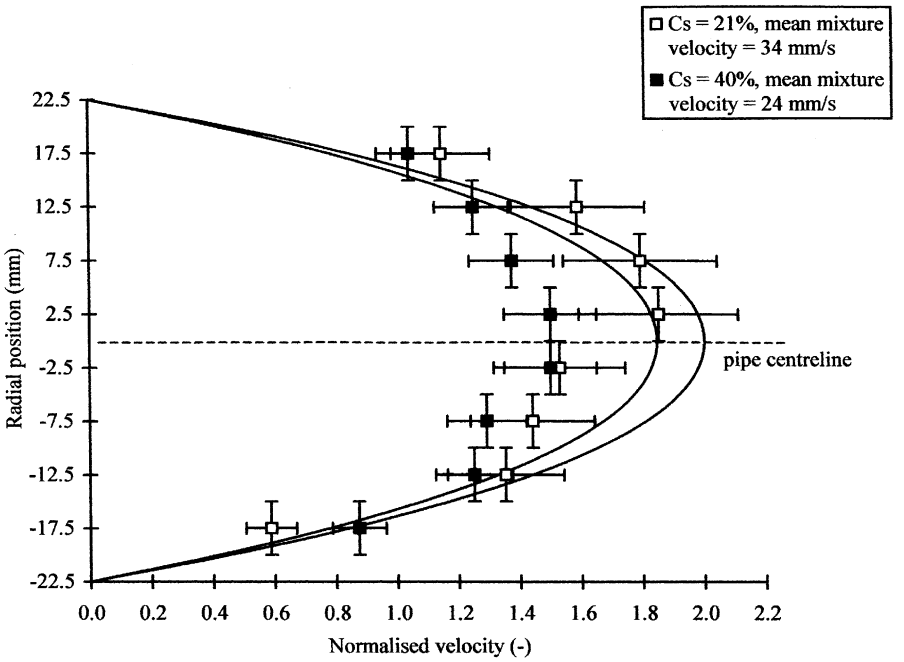

Fig. 10. Vertical plane velocity profiles in horizontal flow: solid lines represent velocity profiles for Ellis liquid flowing alone; 0.8% w/w CMC; $d = 10$ mm.

The skewness parameter, $\overline{s}_n$, defined in Eq. (2) was plotted against the product $CsRe_{\mathrm{pm}}$, where $Re_{\mathrm{pm}}(=\rho_L \overline{v} d/\mu_{\mathrm{a}}^{\mathrm{mean}})$ is a modified particle Reynolds number based on the mean mixture velocity, $\overline{v}$, and the mean apparent viscosity of the carrier fluid, μ_a^{mean}. The mean apparent viscosity was calculated using the procedure outlined in Appendix B. The trend in Fig. 11 suggests that $\overline{s}_n$ varies in an approximately linear manner as a function of $CsRe_{\mathrm{pm}}$. Radial velocity profiles with $CsRe_{\mathrm{pm}} > 4$ were effectively symmetrical, with $\overline{s}_n < 0.15$.

3.3. Comparison of horizontal flow and vertical downflow

The difference between vertical and horizontal flows will result from the effect of gravity which leads to particle sedimentation. Particle trajectories were determined for 10 mm particles in 0.5% w/w CMC, $Cs = 30\%$ and $\overline{v} = 65$ mm/s, in horizontal flow and vertical downflow. For the experimental conditions where $Re_{\mathrm{p}} > 0.08$, as noted earlier, no slow-moving annular region was observed. Particles were seen to move more slowly near the tube wall in both flow directions. Examination of the trajectories showed little radial movement of particles in vertical flow; the lack of gravitational effects in the vertical pipe meant, as expected, that the flow was symmetrical ($\overline{s}_n = 0.16$). In horizontal flow, however, particles at the bottom of the pipe moved slower, with $v_{\mathrm{np}}^{\mathrm{min}} = 0.5$ compared to 1.0 at the top, thus showing the effect of sedimentation. More radial movement was found in the horizontal flow trajectories; a higher fraction of the tracer flows were found in the base of the tube, suggesting a higher particle density in this region.

The radial velocity profiles in both flow directions are compared in Fig. 12. The velocity profiles in vertical downflow were more flattened than in horizontal flow; consequently, a smaller range of velocities were measured ($0.6 < v_{\mathrm{np}} < 1.4$ for horizontal flow, and $0.9 < v_{\mathrm{np}} < 1.2$ for vertical downflow). It would, therefore, on this evidence appear advantageous to use vertical downflow if processing requires plug flow.

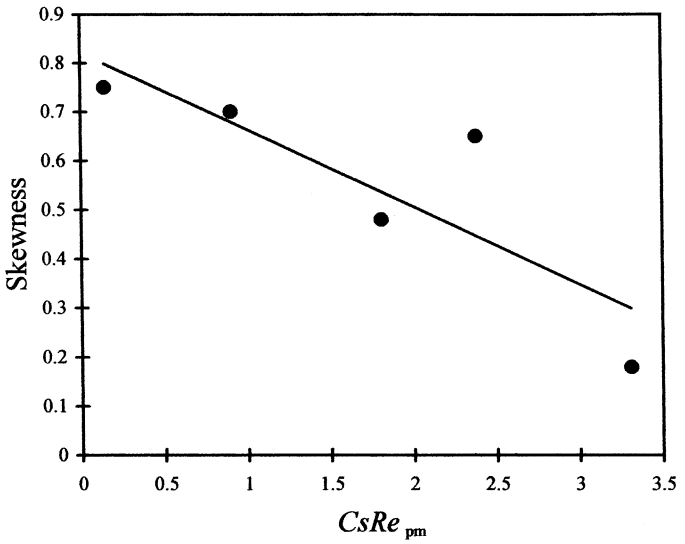

Fig. 11. Skewness of particle radial velocity profiles in horizontal flow as a function of $CsRe_{\mathrm{pm}}$.

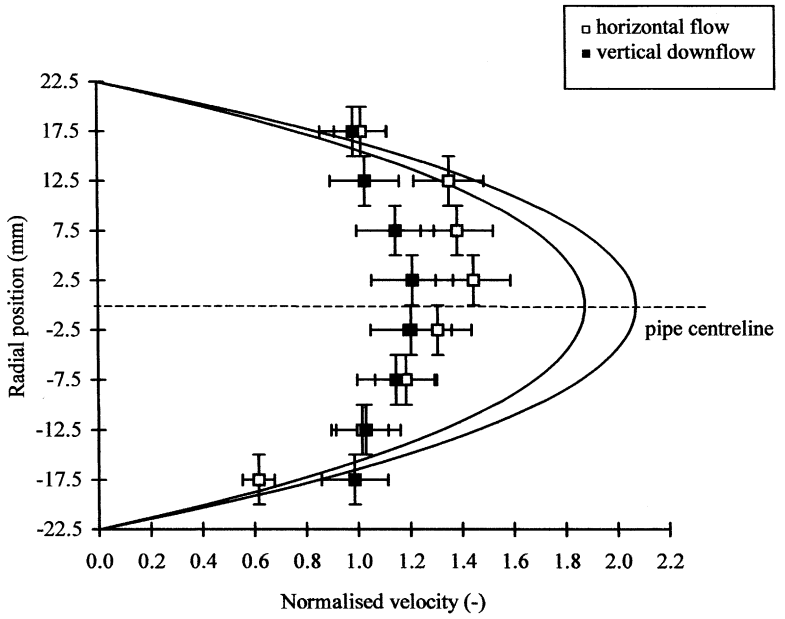

Fig. 12. Particle velocity profiles in horizontal flow and vertical downflow: solid lines represent velocity profiles for Ellis liquid flowing alone; 0.5% w/w CMC; $d = 10$ mm; mean mixing velocity $= 65$ mm/s; $Cs = 30\%$ v/v.

4. Conclusions

The novel method of PEPT has been successfully used to study the behaviour of large nearly neutrally-buoyant particles in high solid concentration pipe flow. PEPT has significant advantages in this type of flow measurement due to the opaque nature of the flows studied, and is thus a useful technique for studying, amongst other flows, the flow of particulate food mixtures. Data can be reported in a number of forms which have been presented here; it is possible to identify individual particle trajectories, statistical velocity distributions and radial velocity profiles. This method gives more detailed results than other methods of studying solid–liquid flows, such as LDA and PIV, because it can look at opaque flows and allows individual tracks to be followed, unlike the use of MRI for example. The techniques developed here have been applied to the study of food flows but they may well be applicable to other types of two-phase flow.

The effects of particle concentration, carrier fluid viscosity, mean mixture velocity, particle size and pipe orientation (horizontal or vertical) on the flow were investigated. The flow pattern depended strongly on particle size, solid concentration and viscosity of the carrier fluid used. When the viscous carrier fluid and/or smaller particles were used, a concentric flow regime with two clearly identifiable flow regions was present: a fast flowing core and a slow moving annular region close to the tube wall, with little particle exchange between regions. These conditions are not ideal for a food flow because they lead to very wide residence time distributions, and thus to significant differences in processing conditions. These experimental conditions could be represented in terms of a particle Reynolds number Re_p; the annular region existed for $Re_p < 0.08$.

As the solid concentration increased from 30% to 40% v/v for 10 mm particles, a transition from concentric to capsule flow was observed. This transition was found to correspond to the maximum solid concentration for which particles could be fitted into two distinct flow regions. The presence of capsules again gives rise to wide variations in particle flow velocity.

The effects of particle sedimentation in horizontal flow could be identified by studying the variation in flow velocity across the pipe. Vertical plane velocity profiles across the pipe were found to be skewed; a skewness parameter was defined which was found to decrease approximately linearly as a function of the product $CsRe_{\mathrm{pm}}$. When this product was greater than 4.0 the radial velocity profiles were found to be essentially axi-symmetric. Velocity profiles in vertical downflow were found to be flatter than in horizontal flow, and hence a smaller range of particle normalised velocities were measured.

The results presented here demonstrate the complexities of flows of large nearly neutrally-buoyant particles in pipes, and that care must be taken in the design of equipment for transport and processing of such mixtures. The work has shown that small changes in experimental conditions can lead to very different flow regimes, and it is an oversimplification to say that plug flow is approached as solid concentration increases. Vertical flows commonly have a narrower range of velocities and may be better than horizontal flows for thermal processing applications.

Appendix A. Particle velocity algorithm

A number of studies have shown that particles can change their radial position in flow (e.g., Lareo et al., 1997a,b); such effects were seen in this work. Particles rapidly changing their radial position will as a consequence give values for their axial velocity which do not reflect the normal velocities at these radii. A data-filtering scheme was thus performed to eliminate velocity data for particles that are rapidly accelerating. The calculation of velocity profiles used 10-point rolling averages: for velocities to be recorded for use in velocity profile data, particles were required to travel at a constant velocity at a constant radial position over at least 10 locations. This is equivalent to a particle trajectory of 5–10 cm.

Initially the PEPT data are presented as a series of (x, y, z, t) co-ordinates. The velocity algorithm used was as follows (assuming that the x axis lies along the tube axis, so that differences in x define the axial velocity):

1. The velocity between successive locations was calculated as

$$v'_i = \frac{x_{i+1} - x_i}{t_{i+1} - t_i}, \tag{A.1}$$

where v'_i is the axial velocity of the particle between the ith and the $(i+1)$th locations, between which the particle moves from x co-ordinate x_i to x_{i+1}, and t_i is the time at which the ith location was made. In the experiments, the distance between successive locations was typically 5–10 mm.

2. A rolling mean for the velocity, $\overline{v}'_i$, was then calculated over 10 points i.e.,

$$\overline{v}'_i = \frac{1}{10} \sum_{j=i}^{j=i+10} \frac{x_{j+1} - x_j}{t_{j+1} - t_j}. \tag{A.2}$$

3. Then the difference in the magnitude in the rolling mean velocity between successive locations was calculated, i.e.,

$$\Delta\overline{v}'_i = \left|\overline{v}'_{i+1} - \overline{v}'_i\right|. \tag{A.3}$$

4. The mean value of $\Delta\overline{v}'_i$ was then calculated over 10 locations i.e.

$$\Delta\overline{v}'_i = \frac{1}{n'}\sum_{i}^{i-10}\Delta v_j, \tag{A.4}$$

$$\langle\Delta\overline{v}'_i\rangle = \frac{1}{10}\sum_{j=i}^{j=i+10}\Delta\overline{v}'_j \tag{A.5}$$

with corresponding to 5–10 cm of particle trajectory. Following this operation, all data where $\langle\Delta\overline{v}'_i\rangle$ was greater than 2 mm/s were discarded. This removed all those events where the change in velocity exceeded this amount, so that the events recorded correspond to particles in a steady state at each radial position.

Appendix B. Calculation of mean apparent viscosity

Since the CMC solutions are shear thinning, apparent viscosities are required. In a non-uniform flow field the apparent viscosity is a function of the radial position. For Ellis model fluids, an apparent viscosity μ_a, based on the wall shear stress τ_w, is often used (Matsuhisa and Bird, 1965), thus:

$$Q = \frac{\pi a^3\tau_w}{4\mu_0}\left[1 + \left(\frac{4}{\alpha+3}\right)\left(\frac{\tau_w}{\tau_{1/2}}\right)^{\alpha-1}\right], \tag{B.1}$$

where Q is the volumetric flow rate, and a the inner pipe radius. The value calculated using Eq. (B.1) will underestimate the mean apparent viscosity in the pipe, because the shear stress is greatest at the tube wall; this can yield erroneous Reynolds numbers. Alternatively, an area-weighted average could be used, thus:

$$\mu_a^{\text{mean}} = \frac{1}{\pi a^2}\int_0^a 2\pi r\mu_a(r)\,\mathrm{d}r \tag{B.2}$$

which after some manipulation gives (Fairhurst, 1998):

$$\mu_a^{\text{mean}} = \frac{\tau_{1/2}^2}{n(\alpha-1)+2}\times\frac{2\mu_0}{\tau_w^2}\sum_0^n\left(\frac{\tau_w}{\tau_{1/2}}\right)^{n(\alpha-1)+2} \tag{B.3}$$

which converges to a single value for $\tau_{1/2} > \tau_w$ as n tends to infinity. The condition $\tau_{1/2} > \tau_w$ was fulfilled under all experimental conditions of carrier fluids and flowrates except for 0.8% w/w CMC at $77 \leqslant \overline{v} \leqslant 230$ mm/s. For these experimental conditions, μ_a was calculated numerically using the value of the mean shear rate in the pipe, $\overline{\dot{\gamma}}$, given by the following equation (Fairhurst, 1998):

$$\overline{\dot{\gamma}} = \frac{1}{\pi a^2}\sum_{i=1}^{20}\dot{\gamma}_i \times 2\pi\left(\frac{r_i + r_{i+1}}{2}\right)(r_i - r_{i+1}), \tag{B.4}$$

where $\dot{\gamma}_i$ is the shear rate acting on annular element i, of which r_i and r_{i+1} are the internal and external radii, respectively. Eq. (B.4) was solved by dividing the velocity field in the pipe into 20 annular elements, and calculating an average shear rate in the pipe by summing the elemental average shear rates weighted by the areas of the elements.

References

Averbakh, A., Shauly, A., Nir, A., Semiat, R., 1997. Slow viscous flows of highly concentrated suspensions – part I: laser-doppler velocimetry in rectangular ducts. Int. J. Multiphase Flow 23, 409–424.

Barigou, M., Mankad, S., Fryer, P.J., 1998. Heat transfer in two-phase solid–liquid food flows: a review. Trans. IChemE, Part C, Food Bioprod. Process. 76, 3–29.

Doron, P., Barnea, D., 1996. Flow pattern maps for solid–liquid flow in pipes. Int. J. Multiphase flow 22, 273–283.

Dutta, B., Sastry, S.K., 1990a. Velocity distributions of food particle suspensions in holding tubes: Experimental and modelling studies on average particle velocities. J. Food Sci. 55, 1448–1453.

Dutta, B., Sastry, S.K., 1990b. Velocity distributions of food particle suspensions in holding tubes: Distribution characteristics and fastest particle velocities. J. Food Sci. 55, 1703–1710.

Fairhurst, P.G., Barigou, M., Fryer, P.J., Pain, J.-P., 1999. Particle passage time distributions in vertical pipe flow of solid–liquid food mixtures. Trans. IChemE, Part C, Food Bioprod. Process. 77, 293–301.

Fairhurst, P.G., Pain, J-P, 1999. Passage time distributions for high solid fraction solid–liquid food mixtures in horizontal flow: unimodal size particle distributions. J. Food Eng. 39, 345–357.

Fairhurst, P.G., 1998. Contribution to the study of the flow behaviour of large nearly neutrally buoyant spheres in non-Newtonian media: application to HTST processing. Ph.D. Thesis, Université de Technologie de Compiègne, France.

Fangary, Y.S., Barigou, M., Seville, J.P.K., Parker, D.J., 2000. Fluid trajectories in a stirred vessel of non-Newtonian liquid using positron emission particle tracking. Chem. Eng. Sci. 55, 5969–5979.

Fregert, J., 1995. Velocity and concentration profiles for a laminar flow for a fluid containing large spheres in a horizontal pipe. Ph.D. Thesis, Lund University, Sweden.

Lareo, C., 1995. The vertical flow of solid–liquid food mixtures. Ph.D. Thesis, Cambridge University, UK.

Lareo, C., Fryer, P.J., Barigou, M., 1997a. The fluid mechanics of two-phase solid–liquid food flows: a review. Trans. IChemE, Part C, Food Bioprod. Process. 75, 73–105.

Lareo, C., Branch, C.A., Fryer, P.J., 1997b. Particle velocity profiles for solid–liquid food flows in vertical pipes: I . single particles. Powder Technol. 93, 23–34.

Lareo, C., Branch, C.A., Fryer, P.J., 1997c. Particle velocity profiles for solid liquid flows: II. Multiple particles. Powder Technol. 93, 35–45.

Liu, S., Pain, J.P., Proctor, J., de Alwis, A.A.P., Fryer, P.J., 1993. An experimental study or particle flow velocities in solid–liquid food mixtures. Chem. Eng. Commun. 124, 97–114.

Matsuhisa, S., Bird, R.B., 1965. Analytical and numerical solutions for laminar flow of the non-Newtonian Ellis fluid. AIChE J. 11 (4), 588–595.

McCarthy, K.L., Kerr, W.L., Kauten, R.J., Walton, J.H., 1997. Velocity profiles of fluid particulate mixtures using MRI. J. Food Process. Eng. 20, 165–177.

McCarthy, K.L., Kerr, W.L., 1998. Rheological characterisation of a model suspension during pipe flow using MRI. J. Food Eng. 37, 11–23.

McKee, S.L., Parker, D.J., Williams, R.A., 1995. Visualisation of size-dependant particle segregation in slurry mixtures using positron emission tomography. In: Frontiers in Industrial Process Tomography, Engineering Foundation, New York, pp. 249–259.

Newitt, D.M., Richardson, J.F., Shook, C.A., 1962. Hydraulic conveying of solids in horizontal pipes. Part II: Distribution of particles and slip velocities. In: Proceedings: Interaction between fluids and particles, IChemE, London, pp. 87–100.

Ohashi, H., Sugawa, T., Kikuchi, K., Henmi, T., 1979. Mass transfer between particles and liquid in solid–liquid two phase up-flow in a vertical tube. J. Chem. Eng. Jpn. 12, 190.

Ohashi, H., Sugawa, T., Kikuchi, K., Ise, M., 1980. Average particle velocity in solid–liquid two-phase flow through vertical and horizontal tubes. J. Chem. Eng. Jpn. 13, 343–349.

Okuda, K., 1981. Trajectory and diffusion of particles in solid–liquid flow of slurry pipeline. J. Pipelines 1, 211–223.

Parker, D.J., Broadbent, C.J., Fowles, P., Hawkesworth, M.R., McNeil, P.A., 1993. Positron emission particle tracking – A technique for studying flow within engineering equipment. Nucl. Instrum. Meth. A 236, 592–607.

Parker, D.J., Dijkstra, A.E., Martin, T.W., Seville, J.P.K., 1997. Positron emission particle tracking studies of spherical particle motion in rotating drums. Chem. Eng. Sci. 52, 2011–2022.

Segner, W.P., Ragusa, T.J., Marcus, C.L., Soutter, E.A., 1989. Biological evaluation of a heat transfer simulation for sterilising low-acid large particle foods for aseptic packaging. J. Food Process. Preserv. 13, 257–274.

Segré, G., Silberberg, A., 1962a. Behaviour of macroscopic rigid spheres in Poiseuille flow. Part 1. Determination of local concentration by statistical analysis of particle passages through cross light beams. J. Fluid Mech. 14, 115–135.

Segré, G., Silberberg, A., 1962b. Behaviour of macroscopic rigid spheres in Poiseuille flow. Part 2. Experimental results and interpretation. J. Fluid Mech. 14, 136–157.

Shauly, A., Averbakh, A., Nir, A., Semiat, R., 1997. Slow viscous flows of highly concentrated suspensions-part II: particle migration, velocity and concentration profiles in rectangular ducts. Int. J. Multiphase Flow 23, 613–616.

Stewart, P.A.E., Rogers, J.D., Skelton, R.T., Slater, P.L., Allen, M.J., Parker, R., Davis, P., Fowles, P., Hawkesworth, M.R., O'Dwyer, M.A., Walker, J., Stephenson, R., 1987. Positron emission tomography – a new technique for observing fluid behaviour in engineering systems. In: Proceedings of the 4th European Conference on Non-destructive Testing, London, Pergamon, Oxford, pp. 2718–2726.

Takeda, Y., 1995. Velocity profile measurement by ultrasonic Doppler method. Exp. Thermal Fluid Sci. 10, 444–453.

Toda, M., Ishikawa, T., Saito, S., Maeda, S., 1973. On the particle velocities in solid–liquid two-phase flow through straight pipes and bends. J. Chem. Eng. Jpn. 6, 140–146.

Tucker, G.S., Withers, P.M., 1994. Determination of residence time distributions of non-settling food particles in viscous food carrier fluids using Hall effect sensors. J. Food Eng. 17, 401–422.

Zitoun, K.B., 1996. Continuous flow of solid–liquid food mixtures during ohmic heating: fluid interstitial velocities, solid area fraction, orientation and rotation. Ph.D. Thesis, Ohio State University, Ohio.